Chen, T., Robinson, L. F., Burke, A., Claxton, L., Hain, M. P., Li, T., Rae, J. W. B., Stewart, J., Knowles, T. D. J., Fornari, D. J., & Harpp, K. S. (2020). Persistently well-ventilated intermediate-depth ocean through the last deglaciation. *Nature Geoscience*, *13*(11), 733-738. https://doi.org/10.1038/s41561-020-0638-6

Persistently well ventilated intermediate depth ocean through the last deglaciation

Tianyu Chen[1,2*], Laura F. Robinson[2], Andrea Burke[3], Louis Claxton[2], Mathis P. Hain[4], Tao Li[1,2], James W.B. Rae[3], Joseph Stewart[2], Timothy D.J. Knowles[5], Daniel J. Fornari[6], Karen S. Harpp[7]

[1]Centre for Marine Geochemistry Research, State Key Laboratory of Mineral Deposits Research, School of Earth Sciences and Engineering, Nanjing University, Nanjing, China

[2]School of Earth Sciences, University of Bristol, Bristol, UK

[3]School of Earth and Environmental Sciences, University of St Andrews, St Andrews, UK

[4]Earth and Planetary Sciences, University of California Santa Cruz, Santa Cruz, USA

[5]School of Chemistry, University of Bristol, Bristol, UK

[6]Department of Geology and Geophysics, Woods Hole Oceanographic Institution Woods Hole, MA, USA

[7]Geology Department, Colgate University, 13 Oak Drive, Hamilton, NY, USA

*Email: tianyuchen@nju.edu.cn

During the last deglaciation (~18 to 11 ka), existing radiocarbon (^{14}C) reconstructions of intermediate waters in the mid to low latitude oceans show widely diverging trends, with some broadly tracking the atmosphere and others suggesting extreme depletions. These discrepancies cloud our understanding of the deglacial carbon cycle because of the diversity of hypotheses needed to explain these diverging records, e.g., injections of ^{14}C-dead geological carbon, mixing of extremely isolated waters from the abyssal ocean, or changes in sites of

deep water ventilation. Here we present absolutely dated deglacial deep-sea coral ^{14}C records of intermediate waters from the Galápagos Platform – in close proximity to the largest reported deglacial ^{14}C depletions – together with data from the low latitude Atlantic. Our records indicate coherent, well-equilibrated intermediate water ^{14}C-ventilation in both oceans relative to the atmosphere throughout the deglaciation. The observed overall trend toward ^{14}C-enriched signatures in our records is largely due to enhanced air-sea carbon isotope exchange efficiency under increasing atmospheric pCO_2. These results suggest that the ^{14}C-depleted signatures from foraminifera are likely sedimentary rather than water mass features, and provide tight ^{14}C constraints for modelling changes in circulation and carbon cycle during the last deglaciation.

Natural radiocarbon is produced in the upper atmosphere, enters the surface ocean via air-sea gas exchange, and is transported to depth by the ocean's meridional overturning circulation. Since ^{14}C decays away with a 5730 year half-life, the ocean's ^{14}C concentration deficit relative to the atmosphere can be used as a chronometer of ocean circulation and a metric of air-sea gas exchange efficiency. Today, the most ^{14}C-depleted signature is found in the deep Northeast Pacific with $\Delta^{14}C$ difference from the pre-bomb atmosphere of ~240 ‰[1]. During the Last Glacial Maximum (LGM, ~22-19 ka), ^{14}C records suggest that large parts of the Pacific and Atlantic were much more ^{14}C-depleted than today, indicative of reduced exchange of carbon between the deep ocean and the atmosphere[2]. This carbon isolation in the deep ocean is thought to

account for much of the drawdown of atmospheric CO_2 at the LGM compared to the preindustrial[3], and results from coupled changes in circulation and biological sequestration of carbon in the deep ocean[4]. The widely held view is that deglacial reinvigoration of ocean overturning brought ^{14}C from the surface to the abyss and at the same time released the ^{14}C-depleted "old" carbon from the deep ocean to the upper ocean and atmosphere.

However, the impact of deglacial overturning circulation on upper ocean ^{14}C ventilation is highly controversial. The presence of anomalously old ^{14}C excursions at intermediate depths during deglaciation has been used as evidence for reconnection of an extremely isolated deep carbon reservoir with the upper ocean (i.e., above the main thermocline) and the atmosphere via Southern Ocean upwelling and Antarctic intermediate waters (AAIW) advection[5]. Other suggested pathways of abyssal carbon release have included ventilation in the North Pacific[6-8] or from the Arctic into the North Atlantic[9]. Alternatively, it has also been proposed that ^{14}C-free carbon from sources such as sub-marine volcanism or methane clathrates were injected into intermediate depths of the ocean, for example in the Eastern Equatorial Pacific (EEP), and may have contributed to the atmospheric CO_2 rise during the last deglaciation[10,11]. Robust reconstructions of ^{14}C at intermediate depths are thus crucial in constraining the nature of deep ocean carbon release to the atmosphere, and potential links to changes in ocean circulation and climate.

Deglacial intermediate water ^{14}C reconstructions

Currently, the available deglacial ^{14}C records from the intermediate depth ocean show a much larger range of variability than deep-ocean or atmospheric records. While some records from benthic foraminifera show anomalies of more than 8000 years from the atmosphere[10], others do not contain any discernible episodes of large ^{14}C-depletion[12-14]. Reliable interpretation of ^{14}C ventilation history for sediment-based records (mainly benthic foraminifera) is critically dependent on age model assumptions. As an example, the same set of benthic ^{14}C data could indicate either a constant modern-like ^{14}C ventilation of deglacial AAIW[12] or a significant decrease in benthic $\Delta^{14}C$ by more than 150‰ during HS1 depending on the choice of age model[15]. Notably, the reported ^{14}C data discrepancies are particularly pronounced in the intermediate waters of the EEP (Figs. 1 and 2, Extended Data Fig. 1), yielding different numbers of occurrences, magnitudes, and durations of ^{14}C-depletion episodes over the last deglaciation. Whilst more recent detrital wood-based chronologies avoid the difficulties of variable surface reservoir ages or uncertainties in age correlation to ice-core/speleothem records, wood-based studies from the EEP also show different magnitudes of ^{14}C-depletions[14,16]. These results make it challenging to obtain a consistent picture of upper ocean ventilation and carbon cycle changes.

As an archive of past seawater chemistry, deep-sea corals can alleviate some of the complications from sedimentary processes, such as bioturbation and diagenesis within restricted pore water environments, because they live above the

89 sediment-water interface. In addition, uranium series ages, which can be determined
90 from their aragonite skeletons, are not influenced by radiocarbon surface reservoir
91 ages or tie-point correlation uncertainties. We present uranium series dated ^{14}C
92 records from two sites at ~600m in the EEP and ~1100 m in the low latitude Atlantic.
93 The deep-sea coral based EEP record largely follows the trajectory of the atmosphere
94 during the deglaciation at the resolution of the data (Fig. 2), and the low latitude
95 Atlantic sample set follows a similar pattern (Extended Data Fig. 1b). Specifically, the
96 coral-based $\Delta^{14}C$ reconstruction of the EEP shows that $\Delta^{14}C$ decreased from 170‰ in
97 early part of the Heinrich Stadial 1 (HS1) to 20‰ in the early Holocene. The
98 proportional offset of $\Delta^{14}C$ relative to the contemporaneous atmosphere ($\Delta\Delta^{14}C_{corr,}$
99 equivalent to previously reported $\Delta^{14}C_{0,adj}$[17], Extended Data Fig. 1, Methods) reveals
100 that our data show no major ^{14}C excursions compared to other published records,
101 some of which show large and variable ^{14}C offsets. When converted to a ^{14}C 'age', the
102 B-Atm age (sample ^{14}C age offset from the contemporary atmosphere) of EEP
103 intermediate waters decreased from ~1300 ^{14}C years in early part of HS1 to ~850 ^{14}C
104 years in the Holocene (Fig. 3e). Much of this change follows the trend expected due
105 to the deglacial increase in atmospheric pCO_2 (Fig. 3a, Methods), which increases the
106 rate of carbon isotope exchange between the atmosphere and the surface ocean[18]. Data
107 from equatorial Atlantic intermediate waters exhibit a broadly similar trend to the
108 EEP, but are consistently better ventilated throughout the last deglaciation by

109 approximately 20-30‰. This difference is small and mostly within the uncertainties
110 of the data (Extended Data Fig. 1b).

111 Our EEP data are in marked contrast with an existing foraminifera-based
112 sediment record also from the Galápagos platform, at virtually the same depth (617
113 m) as our coral-based data (Figs. 1 and 2). The foraminifera-based record shows
114 $\Delta\Delta^{14}C_{corr}$ as low as -670‰[10] (Extended Data Fig. 1d). Given that this excursion is too
115 large to be explained by any recorded deep-water signal, upwelling of carbon from
116 abyssal waters was ruled out, and the release of ^{14}C-free carbon from clathrates or
117 nearby volcanic provinces put forward as a possible mechanism[10]. Due to their close
118 proximity and similar water depths, our data provide strong evidence that the
119 hypothesized geological carbon release did not control the ^{14}C content of intermediate
120 waters near Galápagos. More widely, other foraminifera-based records from the
121 low-latitude eastern Pacific near Baja California show variable degrees of
122 ^{14}C-depletion during the deglaciation, though never reaching values as low as the
123 foraminifera from Galápagos. It hence seems plausible to invoke geologic or aged
124 sedimentary-carbon release into pore waters to explain the foraminiferal ^{14}C
125 anomalies at both Galápagos and Baja California. By contrast, some Baja California
126 benthic ^{14}C records (Extended Data Fig. 1c) are aligned with our deglacial deep-sea
127 coral ^{14}C evolution, further arguing against regionally significant deglacial water mass
128 ^{14}C depletions and in favour of localised offsets in pore waters (Methods). Taking a
129 global view, the absence of any discernible episodes of severe ^{14}C-depletion in our

precisely-dated intermediate-water records suggests that basin-scale ^{14}C-depletion of upper ocean water masses is unlikely to have been prevalent. The relatively well-equilibrated intermediate ^{14}C signatures are in agreement with model predictions[19] and imply short residence time for carbon in the upper ocean due to global air-sea gas exchange similar to the present[19,20].

Well-equilibrated intermediate water ^{14}C ventilation

Today, the ^{14}C signature of the equatorial Atlantic at ~1100 m is similar to the EEP at around ~600 m (Fig. 1). Both sites are fed partly by AAIW, however, a fraction of ^{14}C-enriched NADW entrains into the Equatorial Atlantic intermediate depths, while ^{14}C-depleted North Pacific water contributes a higher proportion to EEP intermediate depths. Modelling and proxy records from the subarctic North Pacific indicate that unlike the modern day, North Pacific convection may have reached below ~2 km in the early deglaciation[6] between 17 and 16 ka, when AMOC was close to a collapsed state[7,21] (Fig. 3b). Our data from the EEP does not exclude the possibility of short-lived deep convection and deep water formation in the North Pacific[7] that brings ^{14}C enriched waters to the abyssal ocean and subsequently to the intermediate EEP. For example, the intermediate water ^{14}C contents of EEP were enriched and were similar to the equatorial Atlantic at ~16.5 ka (Fig. 3e, Extended Fig. 5). Nevertheless, the generally better ^{14}C ventilated signature in the Atlantic records is observed through most of the deglaciation where we have coral-based data.

The coherent signals in the low-latitude coral records from both oceans suggest that our data are representative of the mean ^{14}C evolution of upper ocean waters, after their long-distance advection and mixing from their high latitude sources[19]. Theory and modelling[18,19] suggest that the deglacial pCO_2 increase would have resulted in a greater overall air-sea CO_2 exchange and more complete $^{14}C/C$ equilibration, with an inverse scaling between surface water ^{14}C reservoir ages and pCO_2. The offsets of our data from this simple scaling (baseline in Fig. 3e, Extended Data Fig. 5) are small, suggesting this equilibration mechanism could explain most of the overall deglacial decline in intermediate water B-Atm age without invoking circulation change. In addition to changes in air-sea disequilibrium in the surface ocean, these small B-Atm ^{14}C age excursions can be interpreted as the signature of changes in the overturning of the deep ocean and its influence on the intermediate waters, with the impact of changing atmospheric $\Delta^{14}C$ propagated into the interior ocean being an additional complicating factor (Methods). For example, the decrease of atmospheric $\Delta^{14}C$ during HS1 (Fig. 2) would have left the deep water reservoirs relatively more ^{14}C enriched at the time of their formation (all else being equal) and thus should result in lower B-Atm ages. On the contrary, our record shows a higher B-Atm age than expected from the pCO_2 corrected baseline for the well-resolved equatorial Atlantic (Fig. 3E, Extended Data Fig. 5) from the early (~18 ka) to late (~15-16 ka) HS1, thus pointing toward increased connection of the intermediate waters with isolated deep waters, following reduced NADW formation[21] with increased North Atlantic surface reservoir

ages[22,23], enhanced upwelling of circumpolar deep waters[24] associated with intensified Southern Ocean convection and Southern Hemisphere (SH) westerlies[25], and/or progressively deeper upwelling and ventilation[26]. Subsequently, at the HS1 to B-A transition (i.e., 15-14.6 ka), atmospheric $\Delta^{14}C$ declined more rapidly than the intermediate water records, yielding a trend toward better-ventilated oceanic signatures at low latitudes (Fig. 2a) and possibly recording the influence of enhanced formation of ^{14}C-rich NADW at this time[13,27]. Dedicated ocean modelling work (such as applying the transit-time distribution technique[28]) will be needed to precisely deconvolve the ^{14}C effects of physical circulation change, variable surface ocean disequilibrium, and variable atmosphere ^{14}C propagated into the interior ocean. Our finding that the observed intermediate water $\Delta^{14}C$ in the Atlantic and Pacific largely track atmospheric $\Delta^{14}C$ with a predictable pCO_2-dependent offset will be crucially important in these efforts.

Implications for deglacial carbon cycling

Our study provides unique constraints on oceanic carbon cycle dynamics during the last deglaciation. First, we argue that episodes of anomalous intermediate depth ^{14}C-depletion recorded by benthic foraminifera (Fig. 2, Extended Data Fig. 1) are very likely to be sedimentary rather than global or basin-scale water mass features. The impact of geological carbon on deglacial carbon cycle must therefore be re-evaluated in climate models in light of the new data obtained in this study. Second, due to the precise age control on deep-sea corals, we can resolve a minor excursion in the

well-equilibrated intermediate water ^{14}C records during HS1 (i.e., from ~18 ka to 15-16 ka). This signature is indicative of enhanced mixing of relatively ^{14}C-depleted, presumably carbon-enriched deep reservoirs with the upper ocean during the early deglaciation, consistent with CO_2 outgassing of low latitude upwelling zones[29,30], improved ventilation in the deep Southern Ocean[31] (Fig. 3c), and resulting in atmosphere pCO_2 rise (Fig. 3a). Finally, surface ^{14}C reservoir age variability in the mid-low latitude surface oceans is a consequential and much debated source of uncertainty in dating marine sediment cores based on planktonic foraminifera ^{14}C measurements. Given that surface and thermocline waters are linked by high latitude upwelling and that surface waters have more carbon isotope exchange with the atmosphere than the intermediate waters at any time, the limited apparent ventilation age changes in our coral-based data would require that surface ^{14}C reservoir age variability in the mid-low latitudes should also be limited during the last deglaciation, unless there were substantial changes in local subsurface upwelling. Such understanding is consistent with recent surface (0-100 m) reservoir age simulations which show local variability of less than 500 years in the mid-low latitudes (e.g., 40° S- 40° N) over the last 20 kyr[32]. Overall, our precise reconstruction of intermediate water ^{14}C changes yields powerful constraints on mixing between the deep and upper ocean as well as the ocean carbon cycle at the end of the last ice age.

References

1 Key, R. M. et al. A global ocean carbon climatology: Results from Global Data Analysis Project (GLODAP). *Global Biogeochem. Cycles* **18**, GB4031 (2004).

2 Skinner, L. C. et al. Radiocarbon constraints on the glacial ocean circulation and its impact on atmospheric CO2. *Nat. Commun.* **8**, 16010 (2017).

3 Monnin, E. et al. Atmospheric CO2 concentrations over the last glacial termination. *Science* **291**, 112-114 (2001).

4 Sigman, D. M., Hain, M. P. & Haug, G. H. The polar ocean and glacial cycles in atmospheric CO2 concentration. *Nature* **466**, 47-55 (2010).

5 Marchitto, T. M., Lehman, S. J., Ortiz, J. D., Fluckiger, J. & van Geen, A. Marine radiocarbon evidence for the mechanism of deglacial atmospheric CO(2) rise. *Science* **316**, 1456-1459 (2007).

6 Okazaki, Y. et al. Deepwater Formation in the North Pacific During the Last Glacial Termination. *Science* **329**, 200-204 (2010).

7 Rae, J. W. B. et al. Deep water formation in the North Pacific and deglacial CO_2 rise. *Paleoceanography* **29**, 645-667 (2014).

8 Gray, W. R. et al. Deglacial upwelling, productivity and CO_2 outgassing in the North Pacific Ocean. *Nat. Geosci.* **11**, 340-344 (2018).

9 Thornalley, D. J. R. et al. A warm and poorly ventilated deep Arctic Mediterranean during the last glacial period. *Science* **349**, 706-710 (2015).

10 Stott, L., Southon, J., Timmermann, A. & Koutavas, A. Radiocarbon age anomaly at intermediate water depth in the Pacific Ocean during the last deglaciation. *Paleoceanography* **24**, PA2223 (2009).

11 Stott, L. D., Harazin, K. M. & Krupinski, N. B. Q. Hydrothermal carbon release to the ocean and atmosphere from the eastern equatorial Pacific during the last glacial termination. *Environ. Res. Lett.* **14**, 025007 (2019).

12 De Pol-Holz, R., Keigwin, L., Southon, J., Hebbeln, D. & Mohtadi, M. No signature of abyssal carbon in intermediate waters off Chile during deglaciation. *Nat. Geosci.* **3**, 192-195 (2010).

13 Chen, T. et al. Synchronous centennial abrupt events in the ocean and atmosphere during the last deglaciation. *Science* **349**, 1537-1541 (2015).

14 Zhao, N. & Keigwin, L. D. An atmospheric chronology for the glacial-deglacial Eastern Equatorial Pacific. *Nat. Commun.* **9**, 3077 (2018).

15 Siani, G. et al. Carbon isotope records reveal precise timing of enhanced Southern Ocean upwelling during the last deglaciation. *Nat. Commun.* **4**, 2758 (2013).

16 Rafter, P. A., Herguera, J. C. & Southon, J. R. Extreme lowering of deglacial seawater radiocarbon recorded by both epifaunal and infaunal benthic foraminifera in a wood-dated sediment core. *Clim. Past* **14**, 1977-1989 (2018).

17 Cook, M. S. & Keigwin, L. D. Radiocarbon profiles of the NW Pacific from the LGM and deglaciation: Evaluating ventilation metrics and the effect of uncertain surface reservoir ages. *Paleoceanography*, 2014PA002649 (2015).

18 Galbraith, E. D., Kwon, E. Y., Bianchi, D., Hain, M. P. & Sarmiento, J. L. The impact of atmospheric pCO(2) on carbon isotope ratios of the atmosphere and ocean. *Global Biogeochem. Cycles* **29**, 307-324 (2015).

19 Hain, M. P., Sigman, D. M. & Haug, G. H. Shortcomings of the isolated abyssal reservoir model for deglacial radiocarbon changes in the mid-depth Indo-Pacific Ocean. *Geophys. Res. Lett.* **38**, L04604 (2011).

20 Graven, H., Gruber, N., Key, R., Khatiwala, S. & Giraud, X. Changing controls on oceanic radiocarbon: New insights on shallow□to□deep ocean exchange and anthropogenic CO2 uptake. *J. Geophys. Res. Oceans* **117** (2012).

21 McManus, J. F., Francois, R., Gherardi, J. M., Keigwin, L. D. & Brown-Leger, S. Collapse and rapid resumption of Atlantic meridional circulation linked to deglacial climate changes. *Nature* **428**, 834-837 (2004).

22 Stern, J. V. & Lisiecki, L. E. North Atlantic circulation and reservoir age changes over the past 41,000years. *Geophys. Res. Lett.* **40**, 3693-3697 (2013).

23 Skinner, L. C., Muschitiello, F. & Scrivner, A. E. Marine Reservoir Age Variability Over the Last Deglaciation: Implications for Marine

CarbonCycling and Prospects for Regional Radiocarbon Calibrations. *Paleoceanogr. Paleocl.* **34**, 1807-1815 (2019).

24 Anderson, R. F. et al. Wind-Driven Upwelling in the Southern Ocean and the Deglacial Rise in Atmospheric CO2. *Science* **323**, 1443-1448 (2009).

25 Menviel, L. et al. Southern Hemisphere westerlies as a driver of the early deglacial atmospheric CO2 rise. *Nat. Commun.* **9**, 2503 (2018).

26 Lund, D. C., Tessin, A. C., Hoffman, J. L. & Schmittner, A. Southwest Atlantic watermass evolution during the last deglaciation. *Paleoceanography* **30**, 477–494 (2015).

27 Barker, S., Knorr, G., Vautravers, M. J., Diz, P. & Skinner, L. C. Extreme deepening of the Atlantic overturning circulation during deglaciation. *Nat. Geosci.* **3**, 567-571 (2010).

28 DeVries, T. & Primeau, F. An improved method for estimating water-mass ventilation age from radiocarbon data. *Earth Planet. Sci. Lett.* **295**, 367-378 (2010).

29 Martinez-Boti, M. A. et al. Boron isotope evidence for oceanic carbon dioxide leakage during the last deglaciation. *Nature* **518**, 219-222 (2015).

30 Shao, J. et al. Atmosphere-Ocean CO_2 Exchange Across the Last Deglaciation From the Boron Isotope Proxy. *Paleoceanogr. Paleocl.* **34**, 1650-1670 (2019).

31 Jaccard, S. L., Galbraith, E. D., Martinez-Garcia, A. & Anderson, R. F. Covariation of deep Southern Ocean oxygenation and atmospheric CO2 through the last ice age. *Nature* **530**, 207-210 (2016).

32 Butzin, M., Kohler, P. & Lohmann, G. Marine radiocarbon reservoir age simulations for the past 50,000 years. *Geophys. Res. Lett.* **44**, 8473-8480 (2017).

33 Talley, L. D. Closure of the Global Overturning Circulation Through the Indian, Pacific, and Southern Oceans: Schematics and Transports. *Oceanogr.* **26**, 80-97 (2013).

34 Ingram, B. I., & Kennett, J. P. Radiocarbon chronology and planktonic-benthic foraminiferal 14C age differences in Santa Barbara Basin sediments, Hole 893A. Proceedings of the Ocean Drilling Program, Scientific Results, 146(Part 2), 19–27 (1995).

35 Keigwin, L. D. Late Pleistocene-Holocene paleoceanography and ventilation of the Gulf of California. *J. Oceanogr.* **58**, 421-432 (2002).

36 Lindsay, C. M., Lehman, S. J., Marchitto, T. M., Carriquiry, J. D. & Ortiz, J. D. New constraints on deglacial marine radiocarbon anomalies from a depth transect near Baja California. *Paleoceanography* **31**, 1103-1116 (2016).

37 Umling, N. E. & Thunell, R. C. Synchronous deglacial thermocline and deep-water ventilation in the eastern equatorial Pacific. *Nat. Commun.* **8**, 14203 (2017).

38 Magana, A. L. et al. Resolving the cause of large differences between deglacial benthic foraminifera radiocarbon measurements in Santa Barbara Basin. *Paleoceanography* **25**, PA4102 (2010).

39 Reimer, P. J. et al. Intcal13 and Marine13 Radiocarbon Age Calibration Curves 0-50,000 Years Cal Bp. *Radiocarbon* **55**, 1869-1887 (2013).

40 Marcott, S. A. et al. Centennial-scale changes in the global carbon cycle during the last deglaciation. *Nature* **514**, 616-619 (2014).

41 Burke, A. & Robinson, L. F. The Southern Ocean's Role in Carbon Exchange During the Last Deglaciation. *Science* **335**, 557-561 (2012).

Additional information Correspondence and requests for materials should be addressed to T.C. (tianyuchen@nju.edu.cn).

Acknowledgements This study was funded by the European Research Council, the Natural Environment Research Council (NE/S001743/1; NE/N011716/1), the Philip Leverhulme Trust, the Strategic Priority Research Program of Chinese Academy of Sciences (XDB40010200), National Natural Science Foundation of China (41822603), the U.S. National Science Foundation (OCE-0926637, OCE-10309040, and OCE-0926491), a Marie Curie Reintegration Grant, and the NOAA (National Oceanic and Atmospheric Administration) Ocean Exploration Trust. We also thank the JC094 cruise members, shipboard staff and science party on MV1007 (permit #111-2010), the Charles Darwin Research Station, the Charles Darwin Research Foundation, the

Galápagos National Park, and INOCAR (Instituto Oceanográfico de la Armada de Ecuador) for supporting the coral sampling.

Author Contributions T.C., L.F.R. designed the study and wrote the paper. L.F.R., A.B., D.J.F., K.S.H. collected the deep-sea coral samples. T.C., L.C., T.L., T.D.J.K. did the U-series and ^{14}C analysis. All authors contributed to the discussion on data interpretation and improving the manuscript draft.

Competing interests The authors declare no competing interests.

Figure captions

Fig. 1 Map of sample locations and estimated distribution of pre-bomb ^{14}C concentration. (a) Map showing the selected Pacific-Atlantic transection. (b) Estimated pre-bomb ^{14}C activity of the modern time at water depth of ~700 m[1]. (c) Estimated pre-bomb ^{14}C activity of the Pacific-Atlantic transection[1]. Symbols are sites of this study and existing ^{14}C reconstructions in the mid-low latitudes. Solid arrows indicate circulation of the major global water masses[33]. PDW: Pacific Deep Water; SAMW/AAIW: Subantarctic Mode Water/Antarctic Intermediate Water; UCDW: Upper Circumpolar Deep Water; NADW: North Atlantic Deep Water; AABW: Antarctic Bottom Water.

Fig. 2 The $\Delta^{14}C$ records of the eastern Pacific over the last 20 ky[5,10,12-14,34-38]. IntCal13 shows the atmosphere $\Delta^{14}C$ evolution with $\pm 2\sigma$ uncertainty[39]. Symbols are the same as in Fig.1. 2σ error ellipses of published data and detailed data comparison

354 can be found in Extended Data Fig. 1. YD: Younger Drayes; B-A: Bølling-Allerød;
355 HS1: Henrich Stadial 1.

356 **Fig. 3 The evolution of B-Atm age of our coral records together with other**
357 **paleoclimate reconstructions.** (a) Atmosphere CO_2 concentration[40]; (b) $^{231}Pa/^{230}Th$
358 ratios of sediment core OCE326-GGC5 from the deep subtropical North Atlantic[21];
359 (c) Sedimentary authigenic U concentrations as a deep water oxygenation proxy from
360 a deep Southern Ocean sediment core (TN057-13PC)[31]; (d) B-Atm age evolution of
361 UCDW recorded by deep-sea corals of Drake Passage[13,41]; (e) B-Atm age evolution of
362 low latitude intermediate waters (this study). Dashed green and pink lines represent
363 the scenario with atmosphere pCO_2 as the only factor affecting ^{14}C reservoir age for
364 the EEP and equatorial Atlantic intermediate waters, respectively (Methods). Ellipses
365 and bars show the 2σ uncertainties of the data points. Uncertainties are not shown in
366 case they are smaller than the symbols. B-Atm age: the ^{14}C age difference between
367 sample and the contemporary atmosphere. UCDW: Upper Circumpolar Deep Water.
368
369
370
371
372

METHODS

Materials and analytical methods. The deep-sea corals were collected from the Galápagos platform in the Eastern Equatorial Pacific by both dredging and Remotely Operated Vehicle (ROV) and the low latitude Equatorial Atlantic using by ROV[13,42,43] (Extended Data Figs. 2, 3, 4). Under modern circulation, the studied two sites are in part fed by intermediate/mode water originating from the Southern Ocean, with some inputs from the North Atlantic and North Pacific, so they are well suited to testing hypotheses that link the various pathways of upper-deep ocean mixing and mean state of the upper ocean ventilation. Aragonite deep-sea corals are insensitive to sedimentary processes because they live above the sediment-water interface. Therefore, deep-sea corals can provide a well-constrained ^{14}C activity of bottom water on a precisely dated absolute age scale. In previous deep-sea coral ^{14}C studies of the Southern Ocean[13,41] for example, the generation of ^{14}C temporal evolution is by linking corals growing on different locations and a range of depths, which could potentially incorporate spatial ^{14}C variability in the temporal evolution records. Nevertheless, an obvious strength in this study is that we reconstruct the deglacial ^{14}C ventilation histories using samples essentially growing at the same locations/depths by a single dredge or ROV dive during sample recovery for both oceans. One set of deglacial samples are from the Galápagos Platform recovered from water depth of ~627 m (Fig. 1, Extended Data Figs. 2, 3 and 4, Extended Data Table 1). In addition, we present new data (Extended Data Tables 1 and 2, Extended Data Fig. 6) that fill in

394 a critical gap (late HS1) of an existing ^{14}C record of equatorial Atlantic intermediate
395 waters at water depths of ~1080 m[13]. This composite record is dominated by samples
396 from a single ROV dive at the eastern Atlantic Carter Seamount (EBA), with only a
397 few data points from similar water depths at other seamounts[13] without influencing
398 our data interpretation (Extended Data Fig. 3). Therefore, our samples yield two well
399 resolved, location-bias free, ^{14}C records since the LGM. In both the Pacific and
400 Atlantic, the intermediate waters sampled by our coral-based datasets are part of the
401 upper ocean circulation system and should therefore provide reliable constraints on
402 the release of ^{14}C-depleted carbon from either the deep ocean or geologic sources, as
403 well as on the dissipation of that carbon through the upper ocean and atmosphere.
404 The deep-sea coral from the Galápagos platform are mostly large colonial coral
405 fragments with chunky dense structures. No sign of boring holes or alterations were
406 observed after the samples were cut and cleaned. U-Th ages of the EEP deep-sea
407 corals have been analyzed previously[44]. The intermediate water ^{14}C record of the
408 Equatorial Atlantic is partly based on the published data[13] (i.e., group B of the coral
409 samples in that study). In our study, we have analyzed more samples mainly from the
410 late HS1 based on the age screening results using the LA-MC-ICPMS method
411 developed in the University of Bristol[45]. For U-Th dating of the new coral samples of
412 the equatorial Atlantic, we have followed the method described previously in the
413 same lab[13] and will not be reiterated here. One advantage of the U-Th ages of the
414 coral samples published[13] and new ones in this study is that they were processed in

the same way, and therefore no systematic error is expected between different sets of samples. The ^{14}C data of this study were analyzed by the new AMS facility recently installed in the University of Bristol, while coral ^{14}C data published in Chen et al.[13] were measured in the AMS lab of the University of California, Irvine (UCI). We have re-measured some coral samples that were previously analyzed in UCI. The results (Extended Data Fig. 6, Extended Data Table 3) show that the ^{14}C ages analyzed in Bristol reproduce quite satisfactorily even if coral samples might themselves contain some inhomogeneity. The pretreatment of the coral samples for ^{14}C measurement in Bristol essentially followed the method of UCI. Each coral sample with weight of approximately 15-20 mg was put into a glass tube for acid leach. We have leached the sample to ~10 mg with hot 0.1 N HCl prior to graphitization. After the samples were dried, the samples will react with concentrated phosphoric acid to produce CO_2 which will be transferred into the gas line with helium as the carrier gas to an automated graphitization device. After graphitization, the targets were measured by the MICADAS AMS with acceleration potential of 200 kV. The fossil coral the with ages much older than 50 ka graphitized by the automated device typically give blank ^{14}C ages of 46-50 ka. All data are reported after blank correction with 2 sigma error given in Extended Data Table 1.

Radiocarbon data report. There are three ways to present ^{14}C data in this study. (1) the known-age radiocarbon correction $\Delta^{14}C$, which is expressed as: $\Delta^{14}C_{coral} = (Fm \times e^{(\text{calendar age}/8267)}-1)\times 1000$. (2) To allow direct comparison for the changing atmosphere

436 ^{14}C inventory, deep water ^{14}C is often reported as the B-Atmosphere age, which
437 equals $R_{coral} - R_{atmosphere}$. R_{coral} is the ^{14}C age of corals and $R_{atmosphere}$ is the ^{14}C age of
438 the contemporaneous atmosphere. Error propagation of the uncertainties follows those
439 described previously[13] with a Monte Carlo technique. (3) Offset of deep water $\Delta^{14}C$
440 from the contemporary atmosphere, which is simply as $\Delta\Delta^{14}C=\Delta^{14}C_{coral}$ -
441 $\Delta^{14}C_{atmosphere}$. However, $\Delta\Delta^{14}C$ will change with a changing atmosphere ^{14}C pool,
442 without the true ^{14}C ventilation change. One useful way to apply ^{14}C as a geochemical
443 tracer is to calculate inventory corrected $\Delta\Delta^{14}C_{corr}$[17] which can be expressed as:
444 $\Delta\Delta^{14}C_{corr} = (\exp(\lambda_{Libby}\times(R_{atmosphere} - R_{coral}))-1)*1000$, where λ is the ^{14}C decay constant
445 calculated from the Libby half-life of 5568 years, $R_{atmosphere}$ and R_{coral} are the ^{14}C age
446 of contemporaraneous atmosphere and coral sample, respectively. Note this metric is
447 functionally the same as what was defined elsewhere in the literature such as $\Delta^{14}C_{atm}$
448 $_{normalized}$[46] and ^{14}C[47]. $\Delta\Delta^{14}C_{corr}$ has not corrected the impact of variable atmospheric
449 $\Delta^{14}C$ propagated into the interior ocean. Atmosphere ^{14}C evolution is taken from the
450 IntCal13 calibration curve[39].
451 **Possible causes of EEP ^{14}C depletions.** While there is growing consensus on a more
452 ^{14}C-depleted deep oceans during LGM than today[2,41,47-54], large data scatter is
453 observed at different depths during this period[2]. Radiocarbon data of deep thermocline
454 foraminifera species of the equatorial Atlantic[55] closely track our records, while data
455 of buried deep-sea coral from Brazilian margin show larger scatter[56] (Extended Data
456 Fig. 1d). Deglacial intermediate water ^{14}C data in the mid-low latitude eastern Pacific

457 published over the last 3 decades[5,12,14,34-38,57] show most pronounced variability
458 compared with the deep ocean records (see a recent compilation[58]). It is not yet fully
459 clear what has caused the observed large $\Delta^{14}C$ differences between different records
460 apart from age model uncertainties and bioturbation especially in the intermediate
461 waters. There is indeed pockmark evidence for deglacial releases of clathrates to the
462 overlying water[59], but there is no evidence to support their distinct role in deglacial
463 carbon cycle. Compilation of global occurrences of seep carbonate formation over the
464 last 2 glacial cycles instead implied that enhanced clathrates release occurred during
465 warm high-sea level stands[60]. Regarding hydrothermal carbon contribution to the EEP
466 region, it is likely that diffusion of old carbon from depth did not inject in large
467 quantities to the overlying water mass but remained in the pore waters and at
468 sediment-seawater interfaces, causing large excursions in the benthic foraminifera
469 records without greatly affecting bottom waters. Indeed, negative deglacial excursions
470 of $\delta^{13}C$ are observed in benthic foraminifera records of the EEP with different
471 durations and magnitudes likely linked to pore water chemistry[11,61]. However, it is not
472 possible to reconstruct seawater $\delta^{13}C$ based on the stable carbon isotopes of
473 scleractinian corals because they are strongly regulated by biological vital effects[62].
474 Therefore, our study is unable to provide independent evaluation from the coral stable
475 isotope perspective. Other possibilities such as diagenetic overprint[63] or species
476 effect[38,64] are also worth investigating, but they appear not to be the fundamental
477 causes for benthic foraminifera ^{14}C depletions in the EEP[10,11].

478 ***p*CO$_2$ effect.** *p*CO$_2$ effect describes the phenomenon that atmospheric carbon isotopes
479 exchange more slowly with the seawater when the atmosphere CO$_2$ concentration is
480 lower[18]. This might result in an increase of surface ^{14}C reservoir age by ~250 years,
481 which is then rapidly propagated into the intermediate waters, during the LGM
482 compared to the modern, even when ocean circulation remains invariant. It is
483 important to take this effect into account for our precisely dated coral samples that
484 aim to track nuanced changes in the ocean circulation induced ^{14}C variability of
485 intermediate waters. Rather than introducing new metrics of the ^{14}C to consider the
486 *p*CO$_2$ effect, we simply construct two curves as shown in Fig. 3e with Holocene
487 B-Atm ages of 700 and 900 years, respectively. We then assume all else being equal,
488 and the *p*CO$_2$ effect on ^{14}C reservoir age calculated as: B-Atm $_t$ = B-Atm $_{Holocene}$ *
489 $(pCO_2)_{Holocene}/(pCO_2)_t$[18]. We also have calculated the ^{14}C age offset of each coral
490 record from the two baseline curves, respectively, which is shown in Extended Data
491 Fig. 5.
492 **Effect of variable atmospheric Δ^{14}C propagated into the interior ocean**. The
493 impact of changing atmospheric Δ^{14}C on initial ^{14}C content of deep waters at the time
494 of their formation makes it challenging to deconvolve ocean circulation changes from
495 small B-Atm ^{14}C age excursions. It is interesting to explore whether the small
496 variability in ventilation age of intermediate waters still holds during the last
497 deglaciation when incorporating the influence of variable atmosphere Δ^{14}C
498 propagated into the interior ocean. The projection age technique attempts to measure

499 the time-lag between the entrainment of surface source waters down to greater depths
500 and the time that this $\Delta^{14}C$ is recorded by benthic organisms (e.g., corals or
501 foraminifera, see graphic illustration by Cook et al.[17]). The projection age thus has the
502 potential to take into account the impact of variable atmosphere $\Delta^{14}C$ propagated into
503 the interior ocean. We have calculated the projected age (Extended Data Fig. 7) of the
504 intermediate waters to a hypothetical well-equilibrated surface source (i.e., Marine13
505 calibration curve[39]). In reality, changes in the projection age should reflect combined
506 effects of source water aging and mixing in the deep ocean, as well as variability of
507 the air-sea exchange disequilibrium in the surface ocean. In our study, a higher
508 projection age could mean more isolated, 'older' source waters supplying the
509 intermediate layers, or reduced surface air-sea carbon isotope exchange of the source
510 waters before subducting into the intermediate layers, or a combination of these two
511 effects. Overall, the calculated projection age (Extended Data Fig. 7) has a quite small
512 variability and shows decline by only a few hundred years during the last deglaciation,
513 in corroboration with the understanding based on 'B-Atm age' without considering
514 the impact of variable atmospheric $\Delta^{14}C$ propagated into the interior ocean. In
515 addition, the increasing projection age of the well-resolved Atlantic record from the
516 early (~18 ka) to late HS1 (~15-16 ka) will reinforce our argument on increased
517 mixing of isolated deep waters into the intermediate layers during this period as
518 discussed in the main text. It should be noted that 'projection age' uses a simple
519 assumption about initial ^{14}C signatures of source waters and still could not fully

account for the complexity of various sources of deep waters with different ages[28] supplying the intermediate waters. Nevertheless, the coherency of the understanding from the evolution of 'B-Atm age' and 'projection age' lends strong support to our interpretation on ocean circulation change during HS1.

Data availability Sample location information, U-series ages, and radiocarbon data that support the findings of this study are available in Extended Table 1-3 and also Mendeley Data (http://dx.doi.org/10.17632/vxrmfch8h9.1). The atmosphere CO_2 concentration records, radiocarbon data, $^{231}Pa/^{230}Th$, authigenic uranium flux cited in this study were previously published in refs.[13, 21, 31, 39-41] and are available in the Source Data. The calculated B-Atm age trend without circulation change as well as projection age of the low-latitude coral samples are also available in the Source Data. Detailed information on published foraminifera age and radiocarbon data are available from recent comprehensive compilation[58] (https://www.ncdc.noaa.gov/paleo/study/21390).

References

42 Robinson, L. F. RRS James Cook Cruise JC094, October 13–November 30 2013, Tenerife-Trinidad. TROPICS, Tracing Oceanic Processes using Corals and Sediments. Reconstructing abrupt Changes in Chemistry and Circulation of the Equatorial Atlantic Ocean: Implications for global Climate and deep-water Habitats, *University of Bristol*, (2014).

43 Mittelstaedt, E., Soule, A. S., Harpp, K. S. & Fornari, D. Variations in Crustal Thickness, Plate Rigidity, and Volcanic Processes Throughout the Northern Galápagos Volcanic Province. *Geophys. Monogr. Ser.* **204**, 263 (2014).

44 Chen, T. et al. Ocean mixing and ice-sheet control of seawater U-234/U-238 during the last deglaciation. *Science* **354**, 626-629 (2016).

45 Spooner, P. T., Chen, T., Robinson, L. F. & Coath, C. D. Rapid uranium-series age screening of carbonates by laser ablation mass spectrometry. *Quat. Geochronol.* **31**, 28-39 (2016).

46 Burke, A. et al. The glacial mid-depth radiocarbon bulge and its implications for the overturning circulation. *Paleoceanography* **30**, 1021-1039 (2015).

47 Hines, S. K., Southon, J. R. & Adkins, J. F. A high-resolution record of Southern Ocean intermediate water radiocarbon over the past 30,000 years. *Earth Planet. Sci. Lett.* **432**, 46-58 (2015).

48 Freeman, E., Skinner, L. C., Waelbroeck, C. & Hodell, D. Radiocarbon evidence for enhanced respired carbon storage in the Atlantic at the Last Glacial Maximum. *Nat. Commun.* **7**, 11998 (2016).

49 Keigwin, L. D. & Lehman, S. J. Radiocarbon evidence for a possible abyssal front near 3.1 km in the glacial equatorial Pacific Ocean. *Earth Planet. Sci. Lett.* **425**, 93-104 (2015).

50 Robinson, L. F. et al. Radiocarbon variability in the western North Atlantic during the last deglaciation. *Science* **310**, 1469-1473 (2005).

51 Ronge, T. A. et al. Radiocarbon constraints on the extent and evolution of the South Pacific glacial carbon pool. *Nat. Commun.* **7**, 11487 (2016).

52 Sikes, E. L., Cook, M. S. & Guilderson, T. P. Reduced deep ocean ventilation in the Southern Pacific Ocean during the last glaciation persisted into the deglaciation. *Earth Planet. Sci. Lett.* **438**, 130-138 (2016).

53 Skinner, L. C., Fallon, S., Waelbroeck, C., Michel, E. & Barker, S. Ventilation of the Deep Southern Ocean and Deglacial CO_2 Rise. *Science* **328**, 1147-1151 (2010).

54 Sarnthein, M., Schneider, B. & Grootes, P. M. Peak glacial C-14 ventilation ages suggest major draw-down of carbon into the abyssal ocean. *Clim. Past.* **9**, 2595-2614 (2013).

55 Cléroux, C. & Guilderson, T. Deglacial radiocarbon history of tropical Atlantic thermocline waters: absence of CO_2 reservoir purging signal. *Quat. Sci. Rev.* **30**, 1875-1882 (2011).

56 Mangini, A. et al. Deep sea corals off Brazil verify a poorly ventilated Southern Pacific Ocean during H2, H1 and the Younger Dryas. *Earth Planet. Sci. Lett.* **293**, 269-276 (2010).

57 Bova, S. C., Herbert, T. D. & Altabet, M. A. Ventilation of Northern and Southern Sources of Aged Carbon in the Eastern Equatorial Pacific During the Younger Dryas Rise in Atmospheric CO_2. *Paleoceanogr. Paleocl.* **33**, 1151-1168 (2018).

584 58 Zhao, N., Marchal, O., Keigwin, L., Amrhein, D. & Gebbie, G. A Synthesis of
585 Deglacial Deep-Sea Radiocarbon Records and Their (In)Consistency With
586 Modern Ocean Ventilation. *Paleoceanogr. Paleocl.* **33**, 128-151 (2018).
587 59 Stott, L. et al. CO_2 Release from Pockmarks on the Chatham Rise-Bounty
588 Trough at the Glacial Termination. *Paleoceanogr. Paleocl.* **34**, 1726-1743
589 (2019).
590 60 Chen, F. et al. Gas hydrate dissociation during sea-level highstand inferred
591 from U/Th dating of seep carbonate from the South China Sea. *Geophysical*
592 *Research Letters* **46**, 13928-13938 (2019).
593 61 Bova, S. C. et al. Links between eastern equatorial Pacific stratification and
594 atmospheric CO2 rise during the last deglaciation. *Paleoceanography* **30**,
595 1407-1424 (2015).
596 62 Adkins, J. F., Boyle, E. A., Curry, W. B. & Lutringer, A. Stable isotopes in
597 deep-sea corals and a new mechanism for "vital effects". *Geochim.*
598 *Cosmochim. Ac.* **67**, 1129-1143 (2003).
599 63 Wycech, J., Kelly, D. C. & Marcott, S. Effects of seafloor diagenesis on
600 planktic foraminiferal radiocarbon ages. *Geology* **44**, 551-554 (2016).
601 64 Ezat, M. M. et al. Ventilation history of Nordic Seas overflows during the last
602 (de) glacial period revealed by species-specific benthic foraminiferal 14C
603 dates. *Paleoceanography* **32**, 172-181 (2017).

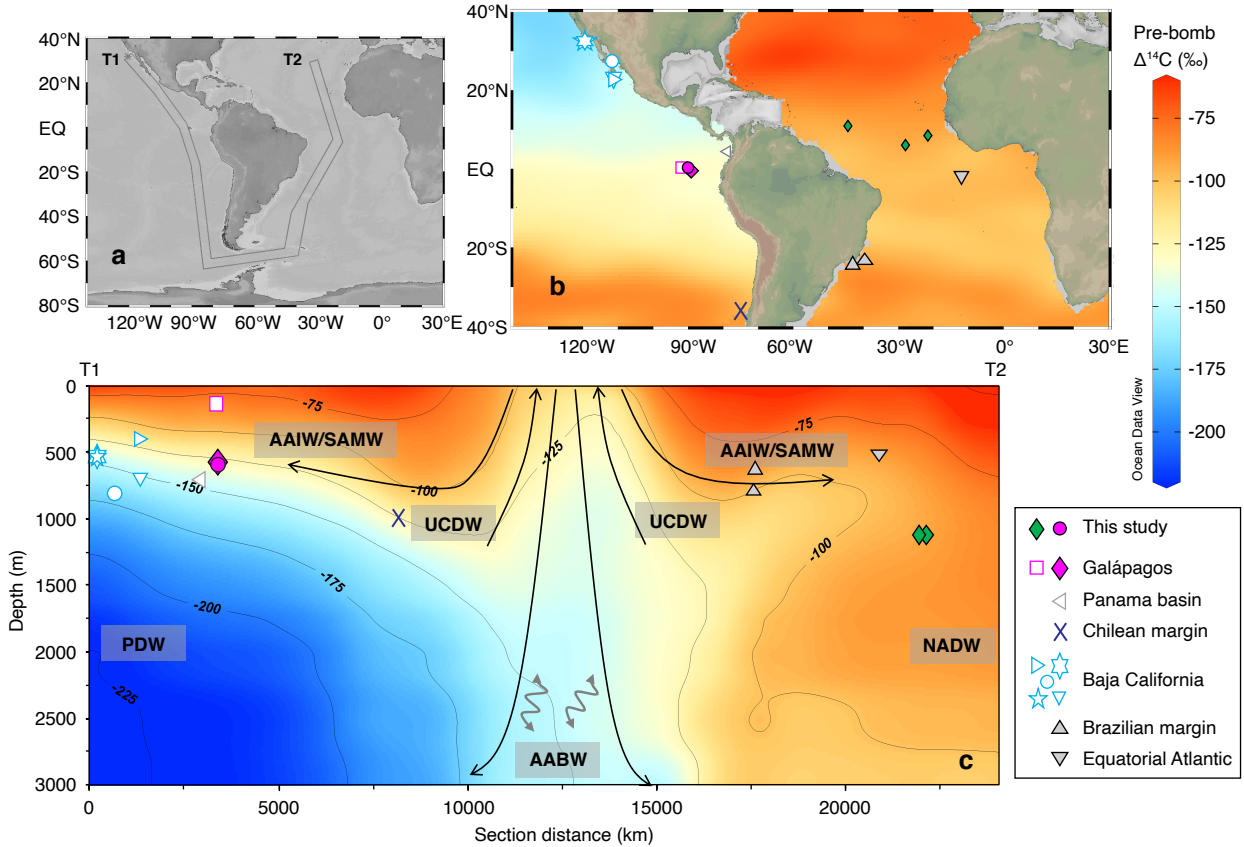
40°N
20°N
EQ
20°S
40°S
60°S
80°S
T1
T2
a
120°W 90°W 60°W 30°W 0° 30°E
b
Pre-bomb
Δ14C (‰)
-75
-100
-125
-150
-175
-200
Ocean Data View
T1
T2
Depth (m)
0
500
1000
1500
2000
2500
3000
AAIW/SAMW
UCDW
PDW
AABW
NADW
c
0
5000
10000
15000
20000
Section distance (km)
This study
Galápagos
Panama basin
Chilean margin
Baja California
Brazilian margin
Equatorial Atlantic

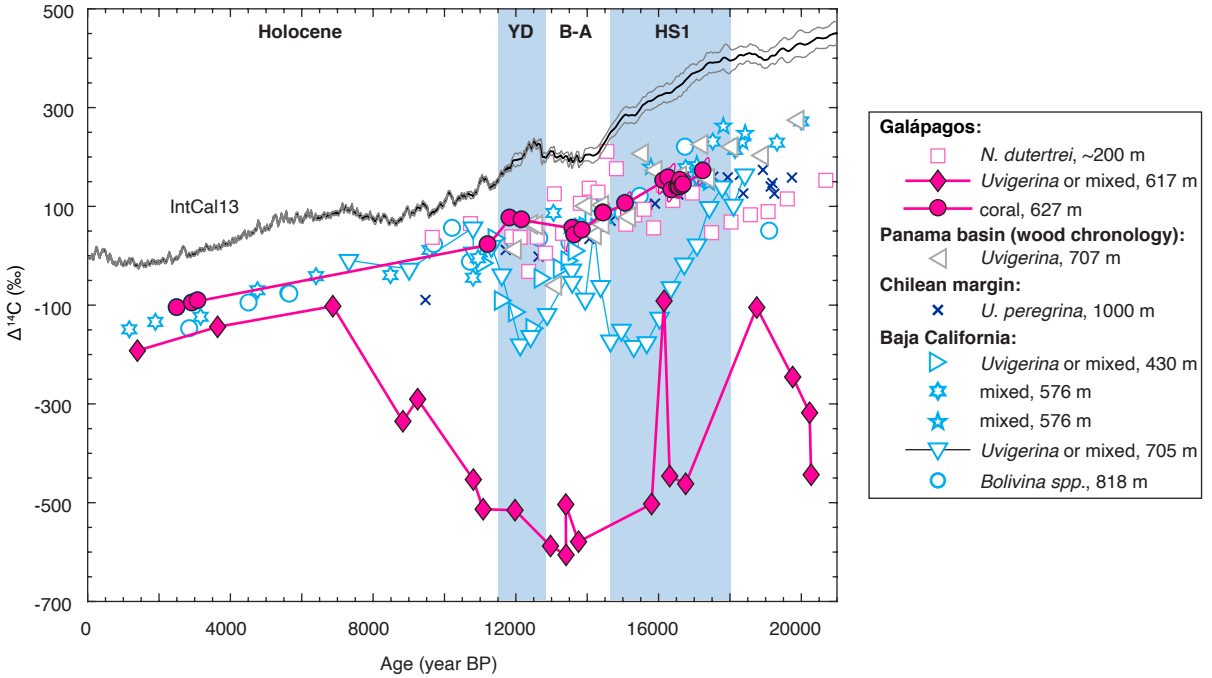
Holocene
YD
B-A
HS1
IntCal13
Δ¹⁴C (‰)
Age (year BP)
500
300
100
-100
-300
-500
-700
0
4000
8000
12000
16000
20000
Galápagos:
N. dutertrei, ~200 m
Uvigerina or mixed, 617 m
coral, 627 m
Panama basin (wood chronology):
Uvigerina, 707 m
Chilean margin:
U. peregrina, 1000 m
Baja California:
Uvigerina or mixed, 430 m
mixed, 576 m
mixed, 576 m
Uvigerina or mixed, 705 m
Bolivina spp., 818 m

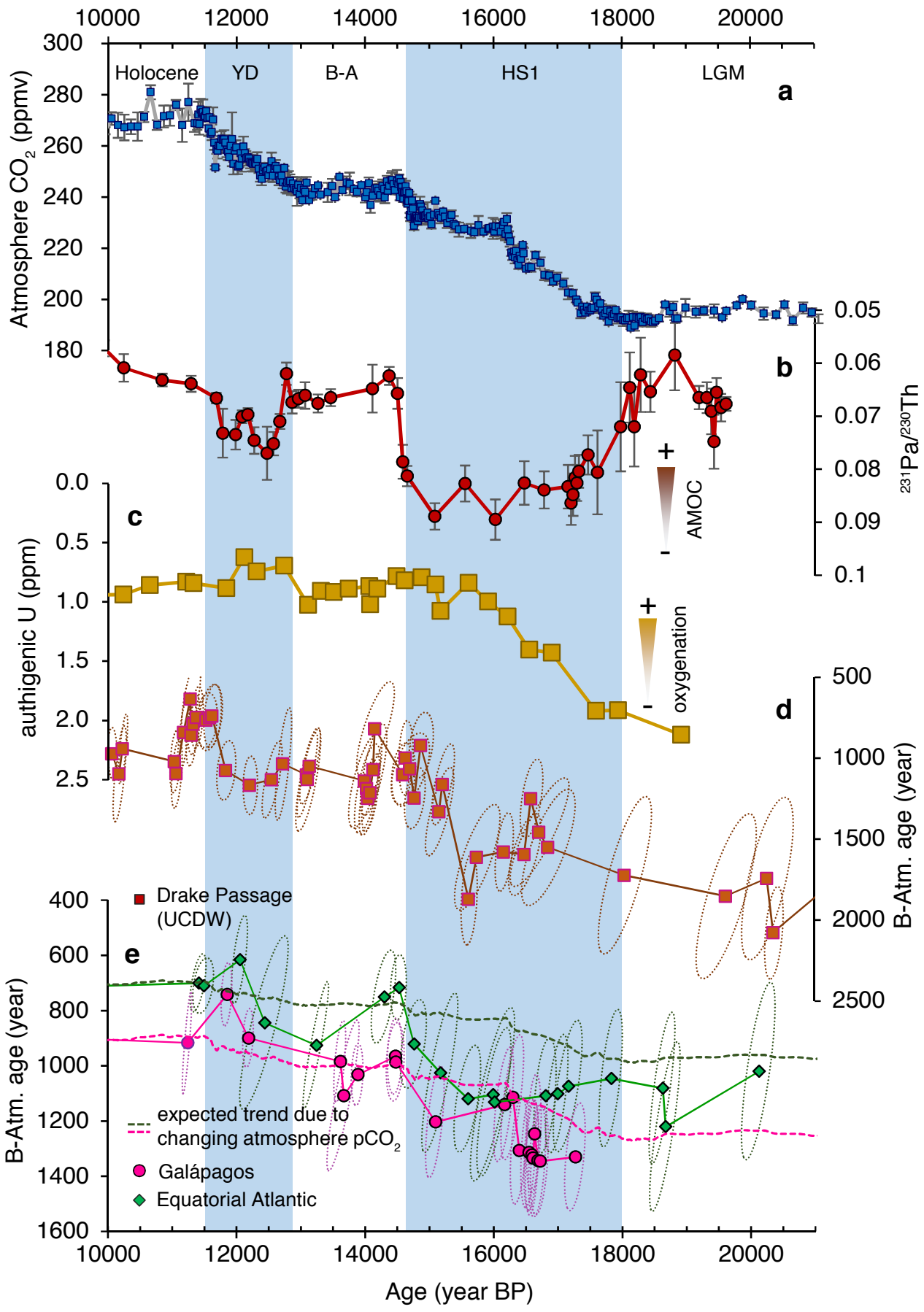
Holocene
YD
B-A
HS1
LGM
a
b
c
d
e
Atmosphere CO2 (ppmv)
231Pa/230Th
AMOC
authigenic U (ppm)
oxygenation
B-Atm. age (year)
Drake Passage (UCDW)
expected trend due to changing atmosphere pCO2
Galápagos
Equatorial Atlantic
Age (year BP)

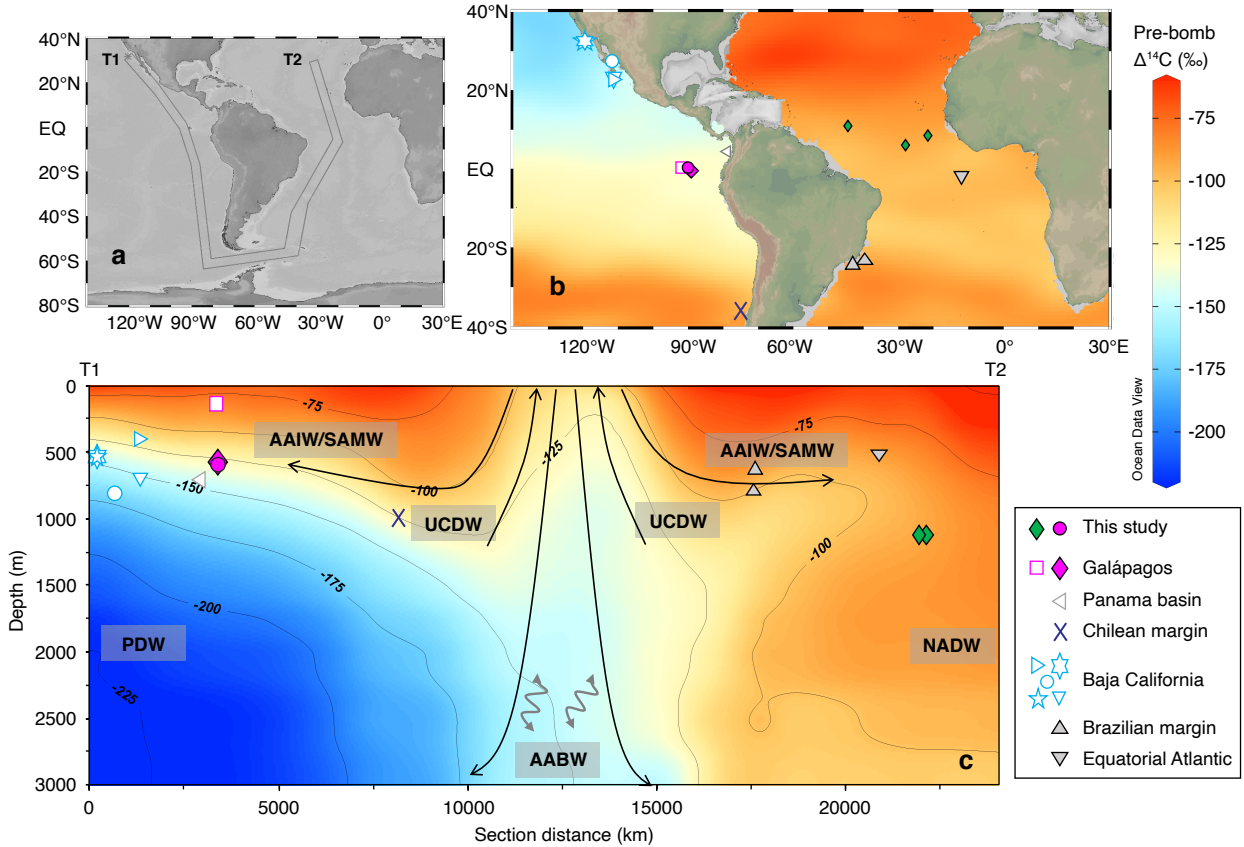
40°N
20°N
EQ
20°S
40°S
60°S
80°S
T1
T2
a
120°W 90°W 60°W 30°W 0° 30°E
b
Pre-bomb
Δ14C (‰)
-75
-100
-125
-150
-175
-200
Ocean Data View
T1
T2
Depth (m)
0
500
1000
1500
2000
2500
3000
AAIW/SAMW
UCDW
PDW
AABW
NADW
c
0
5000
10000
15000
20000
Section distance (km)
This study
Galápagos
Panama basin
Chilean margin
Baja California
Brazilian margin
Equatorial Atlantic

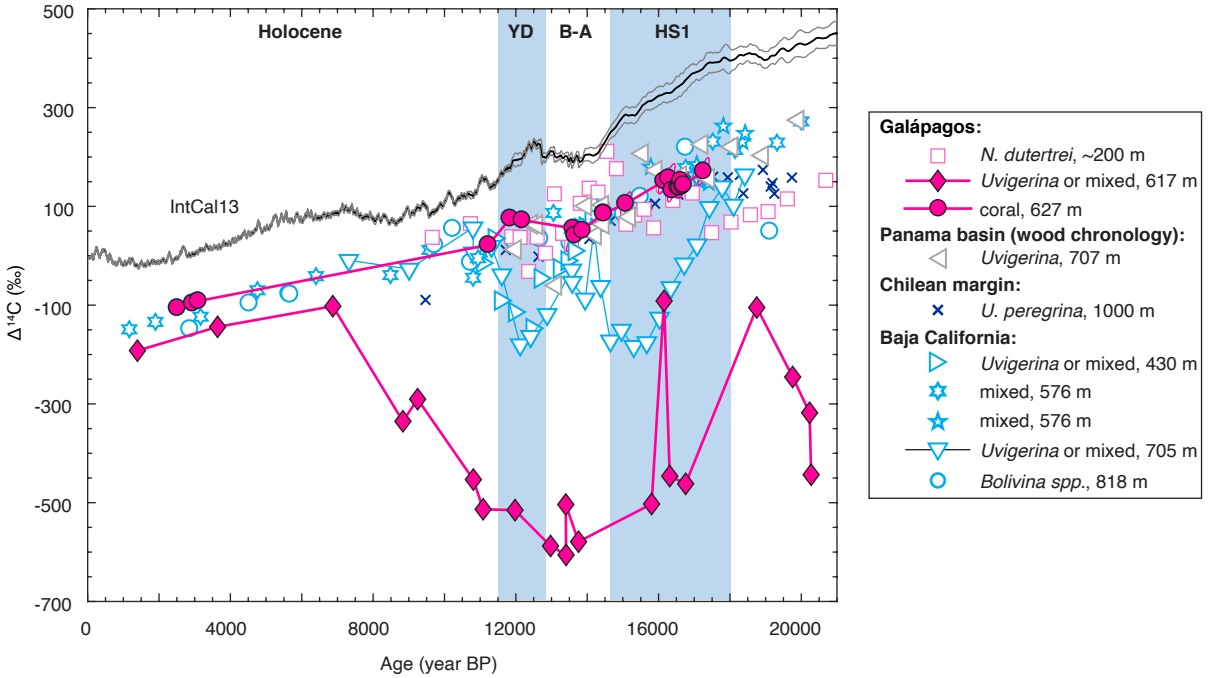
Holocene
YD
B-A
HS1
IntCal13
Δ¹⁴C (‰)
Age (year BP)
500
300
100
-100
-300
-500
-700
0
4000
8000
12000
16000
20000
Galápagos:
N. dutertrei, ~200 m
Uvigerina or mixed, 617 m
coral, 627 m
Panama basin (wood chronology):
Uvigerina, 707 m
Chilean margin:
U. peregrina, 1000 m
Baja California:
Uvigerina or mixed, 430 m
mixed, 576 m
mixed, 576 m
Uvigerina or mixed, 705 m
Bolivina spp., 818 m

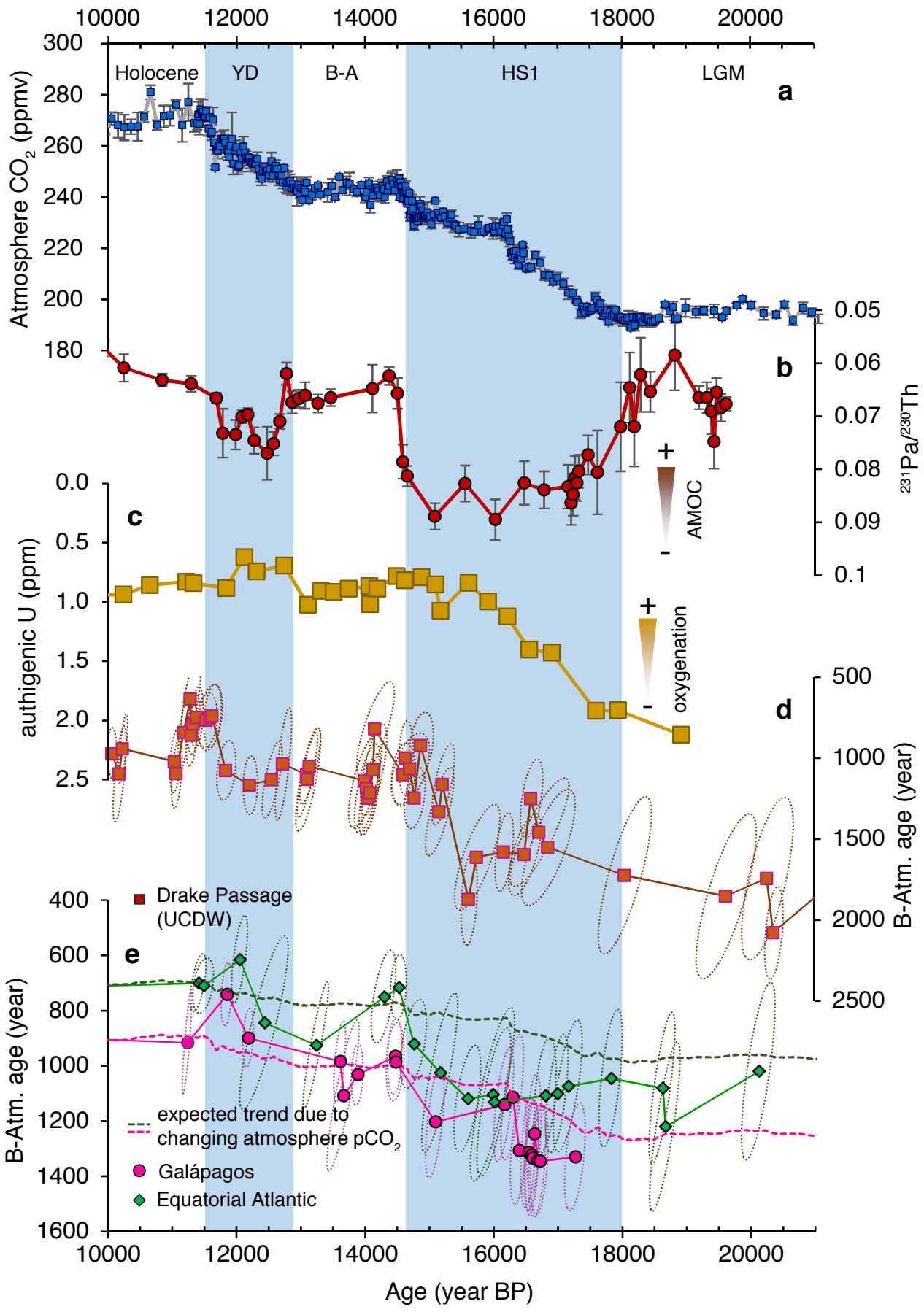
Holocene
YD
B-A
HS1
LGM
a
b
c
d
e
Atmosphere CO2 (ppmv)
231Pa/230Th
AMOC
authigenic U (ppm)
oxygenation
B-Atm. age (year)
Drake Passage (UCDW)
expected trend due to changing atmosphere pCO2
Galápagos
Equatorial Atlantic
Age (year BP)

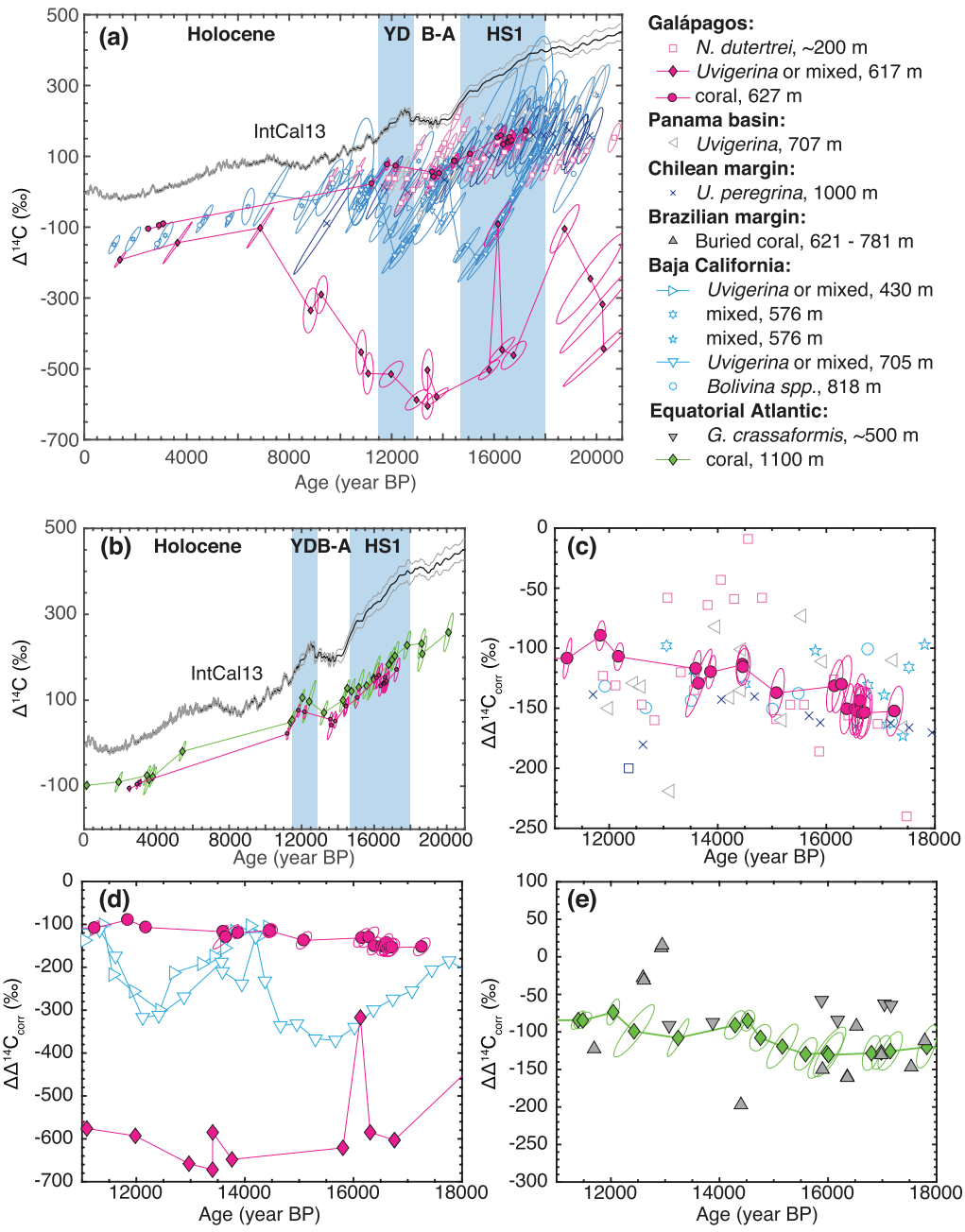
(a)
Holocene
YD
B-A
HS1
IntCal13
Δ14C (‰)
Age (year BP)
Galápagos:
N. dutertrei, ~200 m
Uvigerina or mixed, 617 m
coral, 627 m
Panama basin:
Uvigerina, 707 m
Chilean margin:
U. peregrina, 1000 m
Brazilian margin:
Buried coral, 621 - 781 m
Baja California:
Uvigerina or mixed, 430 m
mixed, 576 m
mixed, 576 m
Uvigerina or mixed, 705 m
Bolivina spp., 818 m
Equatorial Atlantic:
G. crassaformis, ~500 m
coral, 1100 m
(b)
Holocene
YDB-A
HS1
IntCal13
Δ14C (‰)
Age (year BP)
(c)
ΔΔ14Ccorr (‰)
Age (year BP)
(d)
ΔΔ14Ccorr (‰)
Age (year BP)
(e)
ΔΔ14Ccorr (‰)
Age (year BP)

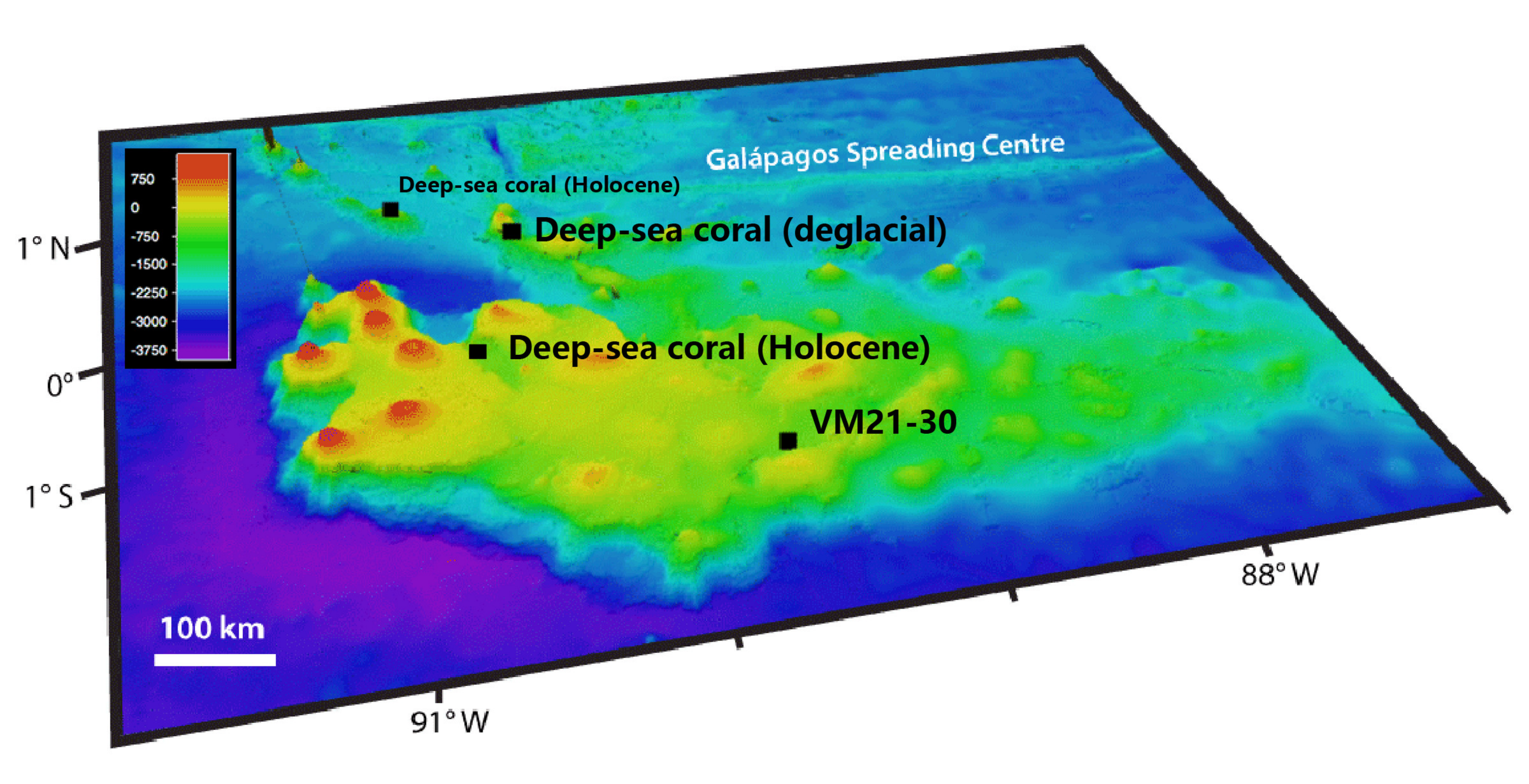
Galápagos Spreading Centre
Deep-sea coral (Holocene)
Deep-sea coral (deglacial)
Deep-sea coral (Holocene)
VM21-30
750
0
-750
-1500
-2250
-3000
-3750
1° N
0°
1° S
91° W
88° W
100 km

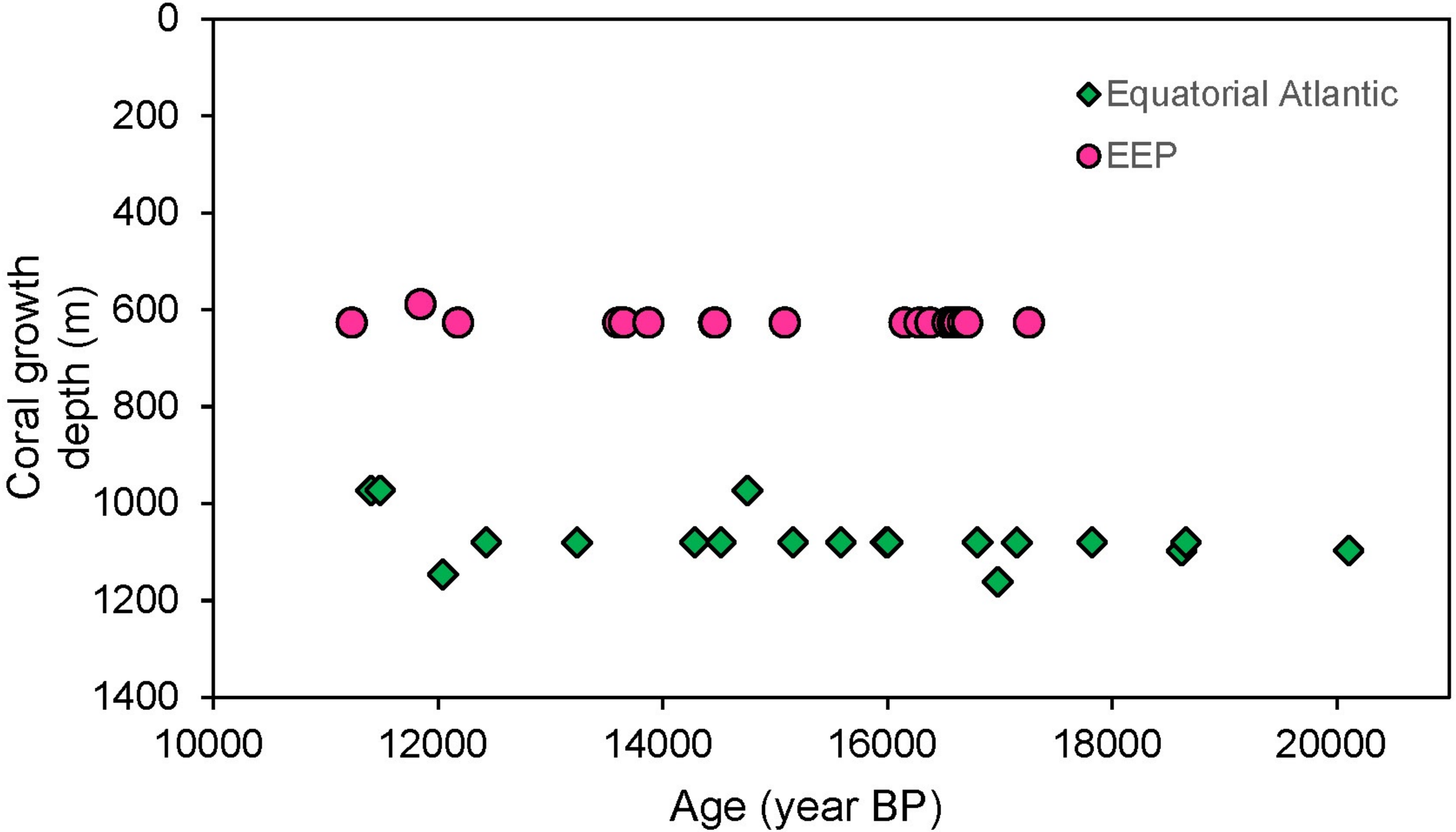
Equatorial Atlantic
EEP
Coral growth depth (m)
0
200
400
600
800
1000
1200
1400
10000
12000
14000
16000
18000
20000
Age (year BP)

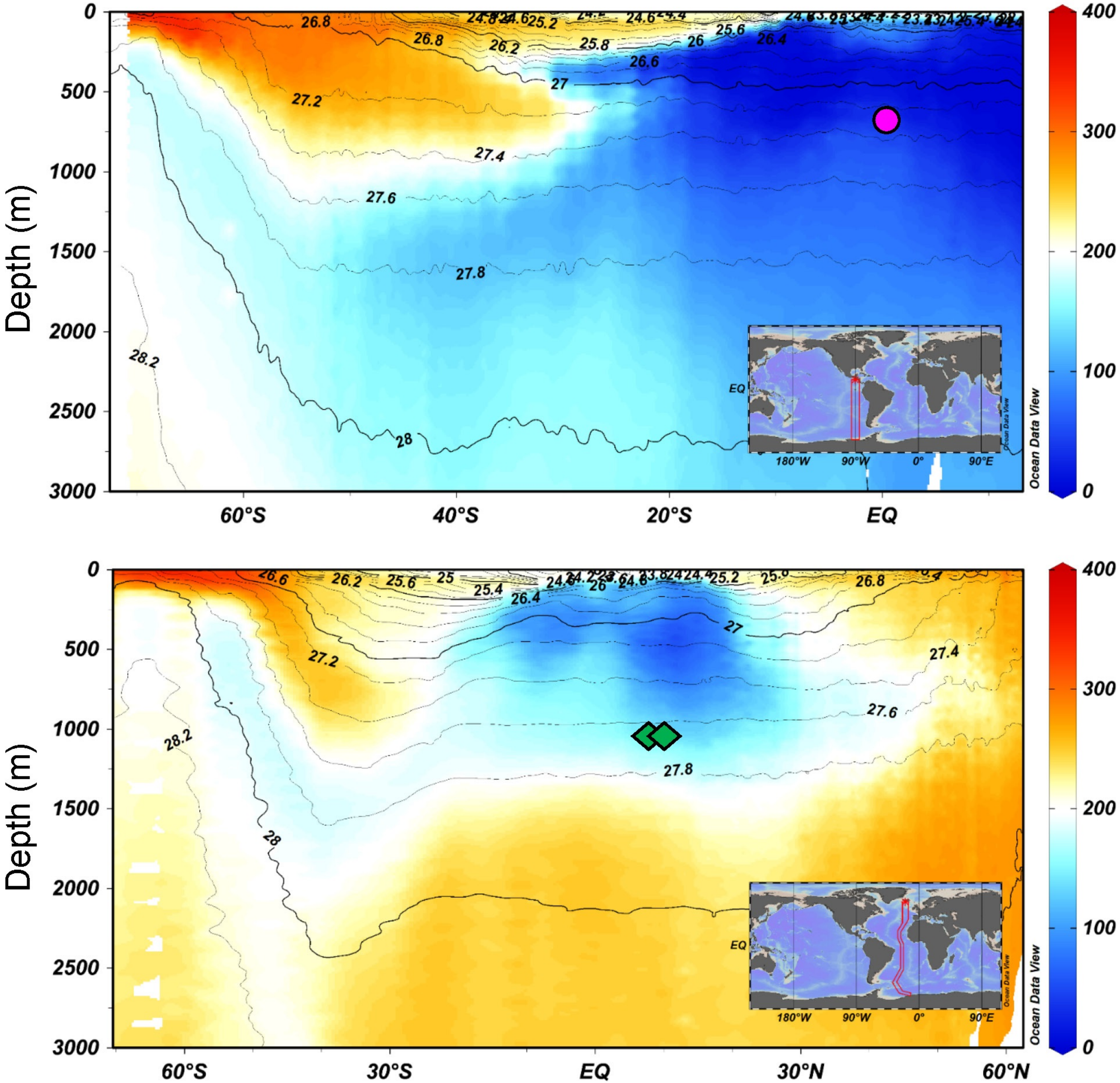
Depth (m)
0
500
1000
1500
2000
2500
3000
60°S
40°S
20°S
EQ
26.8
26.8
26.2
25.8
26
25.6
26.4
26.6
27
27.2
27.4
27.6
27.8
28.2
28
25.2
24.6
24.4
EQ
180°W
90°W
0°
90°E
Ocean Data View
400
300
200
100
0
Ocean Data View
26.6
26.2
25.6
25
25.4
26.4
26
24.6
24.4
25.2
26.8
27
27.2
27.4
27.6
27.8
28.2
28
60°S
30°S
EQ
30°N
60°N
EQ
180°W
90°W
0°
90°E
Ocean Data View
400
300
200
100
0
Ocean Data View

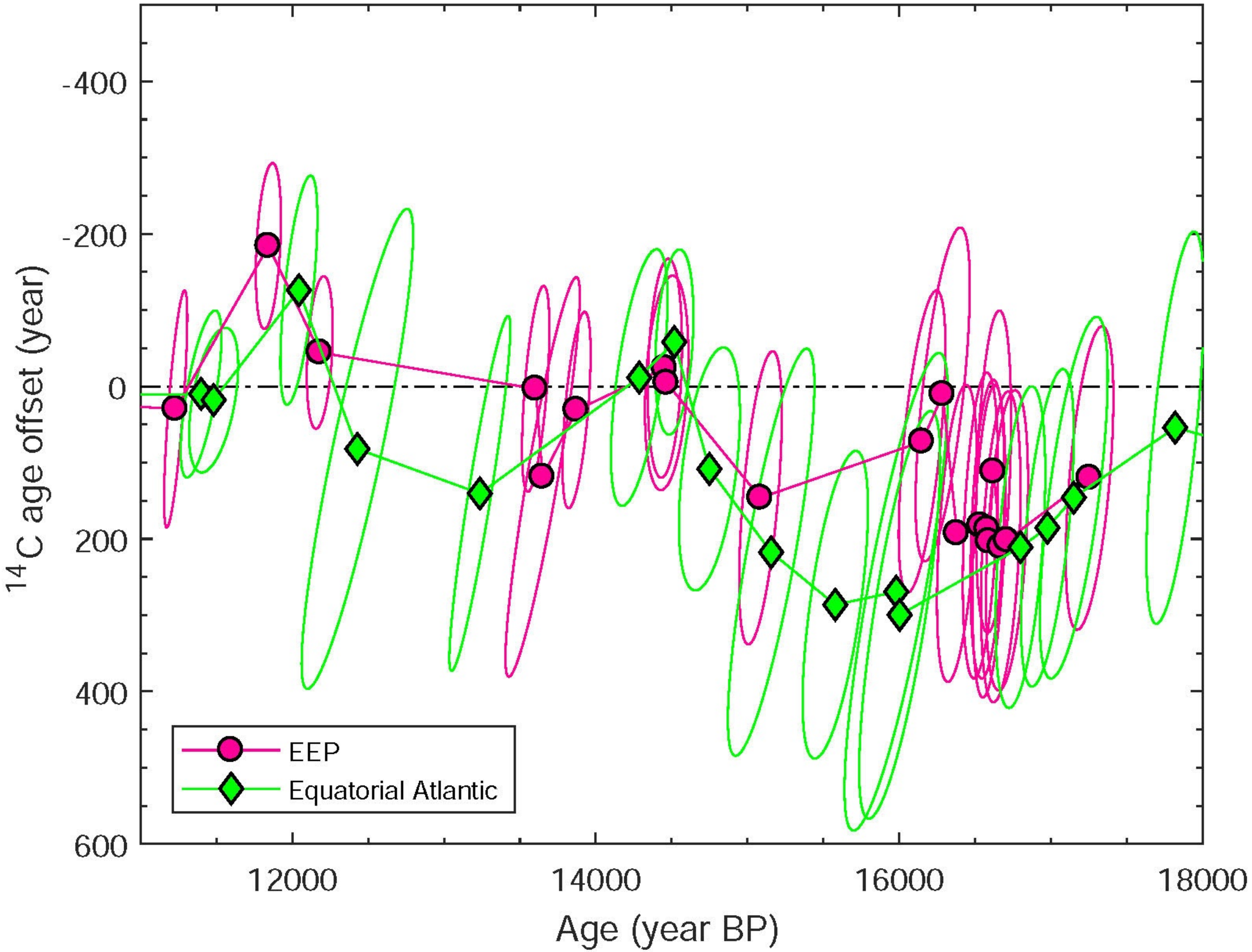
-400
-200
0
200
400
600
^{14}C age offset (year)
12000
14000
16000
18000
Age (year BP)
EEP
Equatorial Atlantic

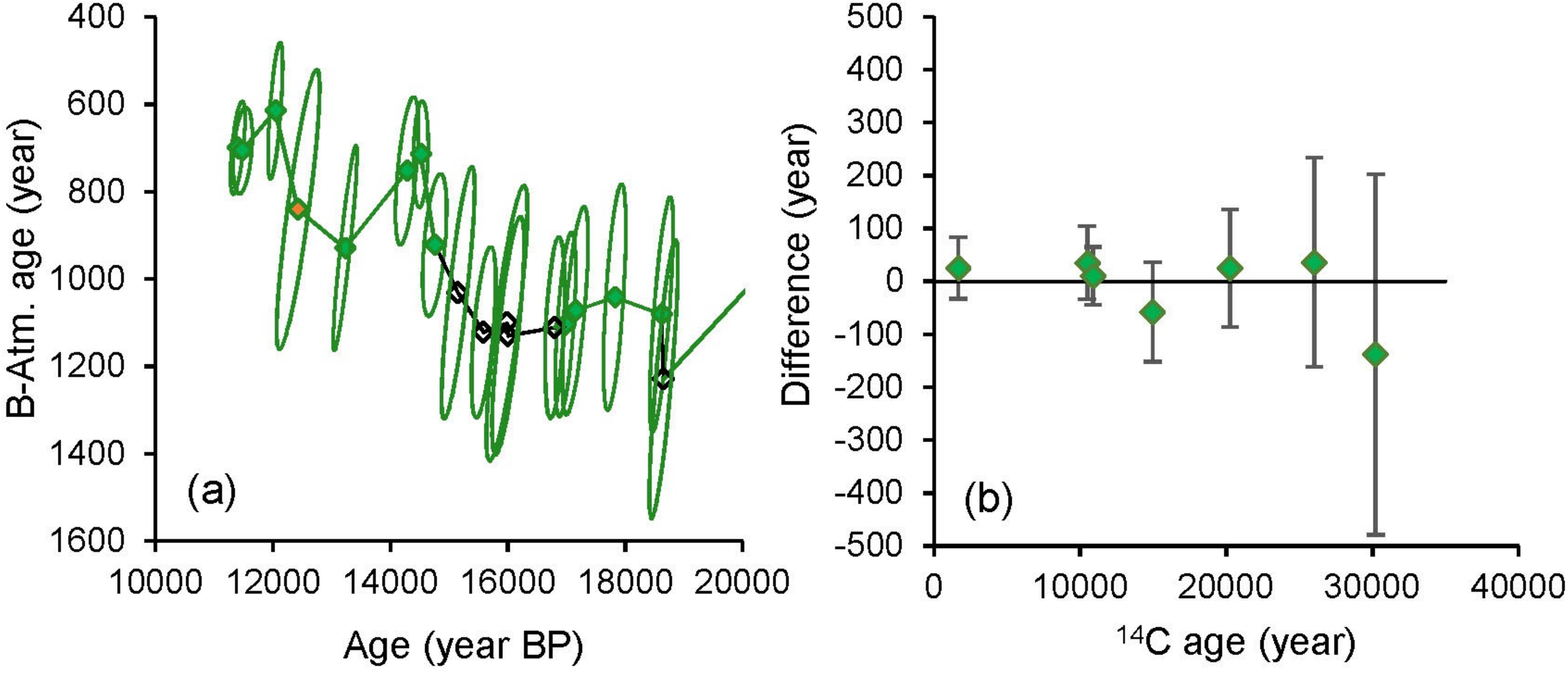
400
600
800
1000
1200
1400
1600
B-Atm. age (year)
(a)
10000
12000
14000
16000
18000
20000
Age (year BP)
500
400
300
200
100
0
-100
-200
-300
-400
-500
Difference (year)
(b)
0
10000
20000
30000
40000
14C age (year)

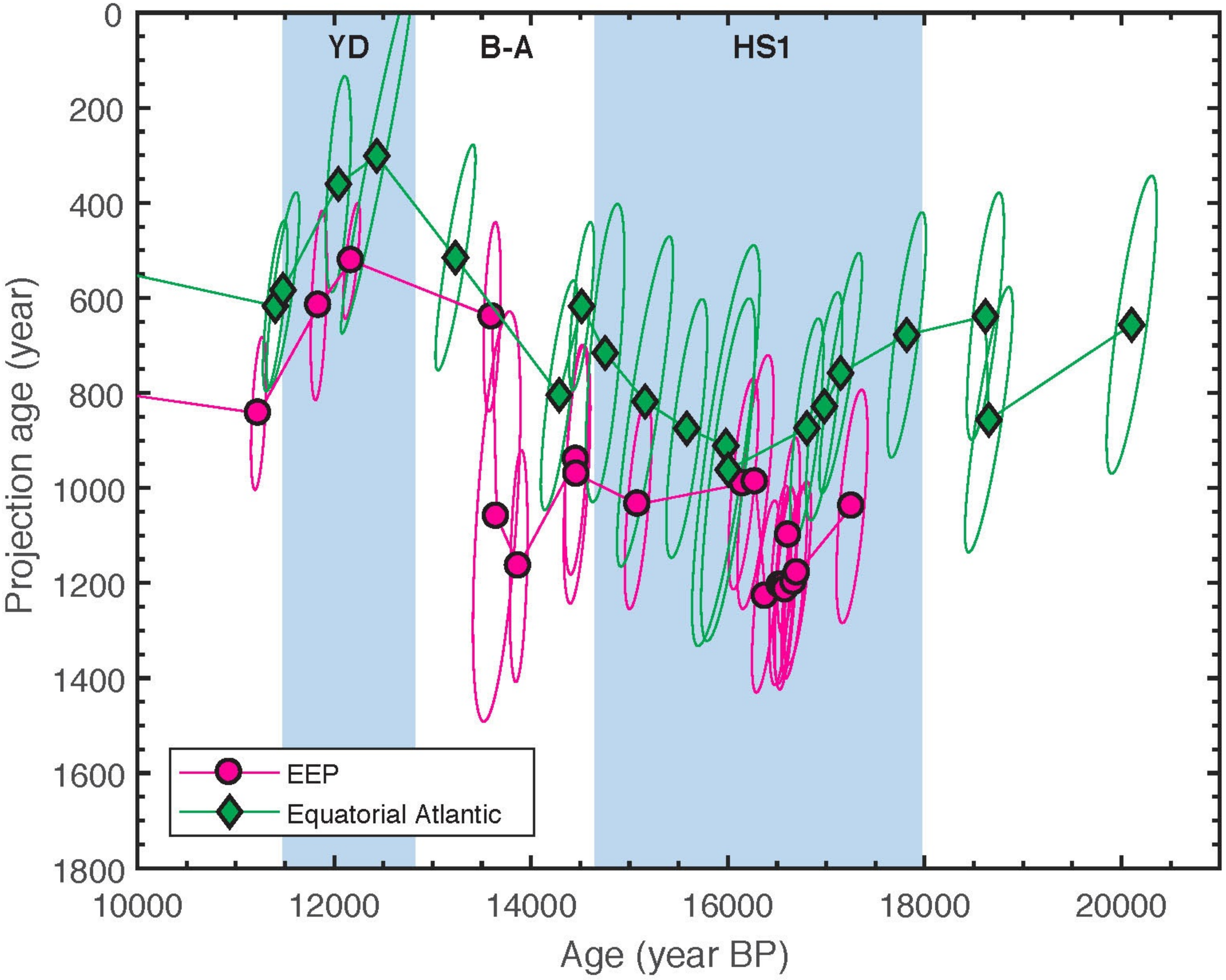
YD
B-A
HS1
0
200
400
600
800
1000
1200
1400
1600
1800
Projection age (year)
10000
12000
14000
16000
18000
20000
Age (year BP)
EEP
Equatorial Atlantic

Region	sample name	Latitude (°N)	Longitude (°E)	Depth (m)	Age (year BP)	2 sigma	^{14}C age	2 sigma	Δ^{14}C (‰)	$\Delta\Delta^{14}$C (‰)	B-Atm (year)
Eq. Atlantic	f0001carcs001	9.216	-21.316	1080	5427	145	5425	59	-19	-94	738
Eq. Atlantic	f0001carcs027	9.216	-21.316	1080	12428	304	11329	67	97	-122	843
Eq. Atlantic	f0001carcs016	9.216	-21.316	1080	15157	230	13747	78	130	-154	1025
Eq. Atlantic	f0001carcs061	9.216	-21.316	1080	15583	167	14128	83	134	-170	1119
Eq. Atlantic	f0001carcs024	9.216	-21.316	1080	15983	284	14392	81	152	-170	1103
Eq. Atlantic	f0001carcs044	9.216	-21.316	1080	16003	220	14435	81	148	-175	1131
Eq. Atlantic	f0001carcs065	9.216	-21.316	1080	16801	138	14972	88	183	-175	1107
Eq. Atlantic	f0001carcs051	9.216	-21.316	1080	18654	198	16606	96	208	-199	1220
Galápagos	MV1007-DO9-19	0.459	-90.712	627	145	17	975	50	-99	-97	818
Galápagos	NA064-118-1-C-2A	-0.371	-90.815	419	2517	21	3343	53	-106	-101	855
Galápagos	NA064-117-01-C-2B	-0.371	-90.815	421	2942	55	3673	53	-96	-99	838
Galápagos	NA064-118-1-C-2B	-0.371	-90.815	419	3101	41	3787	53	-92	-100	841
Galápagos	MV1007-DO3-4-37	0.459	-90.712	627	11231	63	10740	69	22	-123	915
Galápagos	MV1007-DO9-2	0.787	-91.304	589	11843	68	10920	69	76	-104	741
Galápagos	MV1007-DO3-5-16	0.459	-90.712	627	12178	70	11275	71	72	-127	899
Galápagos	MV1007-DO3-4-53	0.459	-90.712	627	13604	74	12788	76	55	-137	984
Galápagos	MV1007-DO3-4-27	0.459	-90.712	627	13654	200	12943	78	41	-155	1107
Galápagos	MV1007-DO3-4-55	0.459	-90.712	627	13873	74	13079	77	51	-144	1031
Galápagos	MV1007-DO3-2-4	0.459	-90.712	627	14458	92	13379	79	87	-139	965
Galápagos	MV1007-DO3-4-60	0.459	-90.712	627	14467	114	13400	79	86	-142	985
Galápagos	MV1007-DO3-4-51	0.459	-90.712	627	15086	118	13852	80	106	-178	1202
Galápagos	MV1007-DO3-4-59	0.459	-90.712	627	16153	129	14559	85	152	-176	1139
Galápagos	MV1007-DO3-4-20	0.459	-90.712	627	16285	150	14650	86	157	-173	1114
Galápagos	MV1007-DO3-2-2	0.459	-90.712	627	16383	106	14919	88	133	-200	1306
Galápagos	MV1007-DO3-2-3	0.459	-90.712	627	16535	93	15021	88	139	-203	1313
Galápagos	MV1007-DO3-2-1	0.459	-90.712	627	16581	92	15059	88	140	-204	1322
Galápagos	MV1007-DO3-4-52	0.459	-90.712	627	16593	91	15082	89	139	-206	1333
Galápagos	MV1007-DO3-2-13	0.459	-90.712	627	16622	92	15009	89	152	-194	1245
Galápagos	MV1007-DO3-2-15	0.459	-90.712	627	16672	109	15140	89	141	-208	1342
Galápagos	MV1007-DO3-5-37	0.459	-90.712	627	16710	111	15158	90	144	-208	1344
Galápagos	MV1007-DO3-4-42	0.459	-90.712	627	17259	127	15507	91	170	-210	1329

sample name	U-Th Age (years) after corr.	2 sigma	U-Th Age (years) before corr.	2 sigma	$\delta^{234}U_{meas}$	2 sigma	$\delta^{234}U_{initial}$	2 sigma	$[^{230}Th/^{238}U]$	2 sigma	^{238}U (ppm)	2 sigma	^{232}Th (ppt)	2 sigma
f0001carcs001	5,493	145	5631	34	146.2	1.0	148.5	1.0	0.0577	0.0003	5.12	0.01	1564	6.48
f0001carcs061	15,649	167	15737	142	144.2	1.2	150.8	1.3	0.1540	0.0013	4.49	0.02	863	5.27
f0001carcs024	16,049	284	16297	138	144.9	1.0	151.6	1.1	0.1592	0.0012	4.40	0.02	2375	12.80
f0001carcs044	16,069	220	16258	109	144.2	1.1	150.9	1.1	0.1587	0.0010	4.36	0.01	1801	8.10
f0001carcs065	16,867	138	16953	107	142.4	1.1	149.4	1.1	0.1648	0.0009	4.48	0.01	839	3.85
f0001carcs051	18,720	198	18854	146	137.8	1.1	145.3	1.1	0.1810	0.0013	4.70	0.01	1367	6.03

sample name	^{14}C age @Bristol (year)	2 sigma	^{14}C age @UCI (year)	2 sigma	Difference (year)	2 sigma
f0076carcs001	1661	52	1636*	39	25	58
f0108carcs003	10490	60	10455*	51	35	69
f0123descm001	10890	54	10880*	50	10	55
f0073carcs001	14949	74	15007*	72	-58	94
f0186carcs005	20243	108	20218*	127	25	111
f0076carcs010	26006	194	25970	240	36	197
f0183carcm001	30212	312	30350	380	-138	341

*Data published in Chen et al.[13]